Thermal and luminescent properties of 2 μm emission in thulium-sensitized holmium-doped silicate-germanate glass

Rong Chen,[1] Ying Tian,[2,*] Bingpeng Li,[1] Xufeng Jing,[2] Junjie Zhang,[1] Shiqing Xu,[1,5] Hellmut Eckert,[3] and Xianghua Zhang[4]

[1]*College of Materials Science and Engineering, China Jiliang University, Hangzhou 310018, China*
[2]*Institute of Optoelectronic Technology, China Jiliang University, Hangzhou 310018, China*
[3]*Institut für Physikalische Chemie, WWU Münster, Corrensstraße 30, D 48149 Münster, Germany*
[4]*Laboratory of Glasses and Ceramics, UMR 6226 CNRS-University of Rennes Cedex 135042, France*
[5]*e-mail: sxucjlu@163.com*
**Corresponding author: tianyingcjlu@163.com*

Received July 6, 2016; revised August 27, 2016; accepted August 27, 2016;
posted September 1, 2016 (Doc. ID 269878); published October 5, 2016

In this paper, we present the luminescent properties of Tm^{3+}/Ho^{3+} co-doped new glass. A series of silicate-germanate glass was prepared by the conventional melt-quenching method. In the Tm^{3+}/Ho^{3+} co-doped silicate-germanate glass, a strong emission of 2 μm originating from the Ho^{3+}:$^5I_7 \rightarrow {}^5I_8$ transition can be observed under conventional 808 nm pumping. The characteristic temperatures, structure, and absorption spectra have been measured. The radiative properties of Ho^{3+} in the prepared glass were calculated. The emission cross section of Ho^{3+} ions transition can reach 4.78×10^{-21} cm^2 around 2 μm, and the FWHM is as high as 153 nm. The energy transfer efficiency between Ho^{3+} and Tm^{3+} has a large value (52%), which indicates the Tm^{3+}/Ho^{3+} co-doped silicate-germanate glass is a suitable candidate for the 2 μm laser. Moreover, the energy transfer mechanism between Tm^{3+} and Ho^{3+} ions was investigated.

OCIS codes: (160.3380) Laser materials; (160.4670) Optical materials; (160.2750) Glass and other amorphous materials; (300.6340) Spectroscopy, infrared.
http://dx.doi.org/10.1364/PRJ.4.000214

1. INTRODUCTION

During the last few decades, the development of solid state lasers generating 2 μm emission has been gaining much attention because of its important applications, such as biomedical uses, mid-infrared remote sensing, monitoring of atmosphere pollutants, eye-safe laser radar, and high-resolution spectroscopy of low-pressure gasses [1–3]. Until now, researchers have made progress in mid-infrared luminescence materials mainly focusing on rare-earth-doped glasses [4,5] and bismuth-doped glasses [6,7]. In order to get a powerful 2 μm laser, it is known that the appropriate selection of rare-earth ions and matrices are important for rare-earth-doped glasses. Ho^{3+} ion can generate a 2 μm laser through transition of Ho^{3+}:$^5I_7 \rightarrow {}^5I_8$, which has been demonstrated in many glass matrices [2,8] until now. However, owing to the absence of a well-matched absorption band, Ho^{3+} cannot directly be pumped by the commercially available 808 or 980 nm laser diode (LD) in single-doped Ho^{3+} systems. In this respect, Tm^{3+}, Er^{3+}, or Yb^{3+} ions were widely added into Ho^{3+}-doped glasses as a sensitizer to achieve 2 μm emission [2,8,9]. Compared with Yb^{3+} and Er^{3+}, Tm^{3+} ions often act as a sensitizer when co-doped with Ho^{3+} ions because the energy gap between Tm^{3+}:$^3F_4 \rightarrow {}^3H_6$ matches with that of Ho^{3+}:$^5I_8 \rightarrow {}^5I_7$. Thus, pump energy can be absorbed by Tm^{3+} effectively and ensuing efficient energy transition from $^3F_4$ of Tm^{3+} to Ho^{3+}:$^5I_7$ under 800 nm LD pumping. Thus, Ho^{3+} can be co-doped with Tm^{3+} ion as a sensitizer, which is a suitable way to achieve 2 μm emission and can be pumped in the wavelength range of commercial LDs.

To obtain a high-efficient mid-infrared emission, host material is another important factor that should be taken into consideration. Up to now, crystals and glasses have been investigated for a 2 μm laser [10–12]. Generally, glasses have the advantage of lower cost and shorter preparation period than those of the crystals [13]. Recent decades have witnessed the development of various Tm^{3+}/Ho^{3+} co-doped glass hosts, including bismuthate glass [9], tellurite glass [14], silicate glass [15], and germanate glass [16] pumped by the common 808 nm LD. To our knowledge, there are some investigations on Er^{3+}/Ho^{3+}-co-doped germanosilicate glass [17], and other investigations were on upconversion luminescence [18]. However, to the best of our knowledge, few researchers have reported on Tm^{3+}/Ho^{3+} double-doped silicate-germanate glass for Raman spectra and 2 μm emission. Silicate-germanate glass combines the advantage of low cost, stable chemical properties of silicate glasses and good thermal stability, relatively low phonon energy together with high infrared transmissivity of germanate glass [19,20]. According to previous reports, we can observe that the vibrational strength of Si-O bonding becomes weaker, and silicate-germanate glass possesses moderate phonon energy due to GeO_2 in substitution for SiO_2 [21]. Therefore, the present paper proposes silicate-germanate glass as the host material.

To the best of our knowledge, there are few studies on Raman spectra, and 2 μm emissions in Tm^{3+}/Ho^{3+} co-doped silicate-germanate glasses have been reported. In the present study, the Raman spectrum in Tm^{3+}/Ho^{3+} co-doped silicate-germanate glass has been investigated. The spectroscopic properties of the silicate-germanate glasses were presented and investigated systematically. According to the Judd–Ofelt (J-O) theory and absorption spectra, J-O parameters, radiative transition probabilities, branching ratios, and lifetimes of Ho^{3+} were calculated in silicate-germanate glass. Furthermore, the related energy-transfer mechanisms among excited states and micro-parameters of the energy transfer processes also were quantitatively analyzed.

2. EXPERIMENTAL

A. Material Synthesis

The molar composition of rare-earth-ions un-doped samples are named SG and S0. Additionally, the investigated glass compositions are shown in Table 1. All the samples were prepared by the conventional melt-quenching method with high purity reagents in powder form. Batches of the samples (20 g) were completely mixed. Then, the samples were placed in a platinum crucible and melted at 1450°C for 30 min until bubble-free liquid was formed. Then, the melts were swirled to ensure homogeneity and subsequently poured on a preheated copper mold and annealed at 550°C for 2 h to remove the internal stresses before they were cooled to room temperature with a muffle furnace. The annealed glass samples have smooth morphology; further, the prepared samples were cut and polished to the size of 10 mm × 10 mm × 1.5 mm for measuring their optical and spectroscopic properties, whereas others were cut and polished for recording refractive index.

B. Measurements

The density of the samples was measured using Archimedes' water-immersion method on an analytical balance. Refractive index was measured at room temperature by the prism minimum deviation method. The characteristic temperatures (temperature of glass transition T_g and onset crystallization peak T_x) were tested by a differential scanning calorimeter (DSC). Absorption spectra were recorded at room temperature in the wavelength range of 350–2200 nm with a Perkin Elmer Lambda 900UV-VIS-NIR spectrophotometer. The Raman spectrum of glass sample was measured with an FT Raman spectrophotometer (Nicolet MODULE) in the spectral range of 60–1100 cm^{-1}, which has a resolution of 4 cm^{-1}. The fluorescence spectra were measured with a computer-controlled Triax 320 type spectrometer upon excitation at 808 nm. The fluorescence lifetimes of $^3F_4$ level were recorded with an HP546800B 100-MHz digital oscilloscope and pumped by 800 nm LD. All the measurements were done at room temperature.

3. RESULTS AND DISCUSSION

A. Physical and Thermal Property

The physical and thermal property results of the analyzed glasses are listed in Table 2. For the investigated samples from Table 2, the density of the germanium-oxide-free sample is found to be 3.16 g/cm^3. Subsequently, it is observed that the density increased after introducing GeO_2 into the glass contents. The reason for increment in density is due to the large molecular weight M of GeO_2. Additionally, the refractive index for the studied compositions also increased with increasing GeO_2 contents. The present silicate-germanate glasses have a high refractive index ($n = 1.70$) compared with fluorophosphate ($n = 1.56$) [8] or silicate ($n = 1.48$) glasses [22]. The rare-earth-ions' electric dipole transition rate A_{rad} increases with the increase of refractive index according to $A_{rad} \sim (n^2 + 2)^2/n$. Thus a higher value of the refractive index (n) increases the spontaneous emission probability (A_{rad}) and consequently provides a better opportunity to obtain laser actions in the laser medium.

At the same time, Table 2 shows the characteristic temperatures (containing temperatures of glass transition T_g and onset crystallization T_x) of the prepared host glass. From Table 2, it can be seen that the present silicate-germanate glass possesses a larger T_g value compared with germanate (596°C) [23] and fluorogallate (640°C) glass [24]. According to previous reports, glass hosts have a high T_g value, which can make it achieve good thermal stability to resist thermal damage at high pumping power [25]. The difference between T_g and T_x($\Delta T = T_x - T_g$) [26] of glass is also given in Table 2. Generally, it is desired that ΔT is as large as possible to achieve a wide range of working temperature during the fiber fabricating. Because fiber fabricating is a reheating process, any crystallization during the process will affect the optical properties [27]. The larger ΔT is, the better thermal stability the glasses will have [28]. According to Table 2, the ΔT of silicate-germanate glass is 155°C, which is significantly higher than that of germanate (111°C) [23] and fluoride (90°C) glass [29]. Thus, the results show that the Tm^{3+}/Ho^{3+} co-doped silicate-germanate glass has good thermal stability, which is helpful for the construction of optical fibers.

Table 1. Compositions of the Prepared Glasses

Samples	Glass Compositions (mol%)
S0	60 SiO_2-20($CaO + Li_2O$)-5Nb_2O_5-15BaO
SG	30 SiO_2-30 GeO_2-20($CaO + Li_2O$)-5Nb_2O_5-15BaO
SGT1	30 SiO_2-30 GeO_2-20($CaO + Li_2O$)-5Nb_2O_5-15BaO -0.5Tm_2O_3
SGT2	30 SiO_2-30 GeO_2-20($CaO + Li_2O$)-5Nb_2O_5-15BaO -1.5Tm_2O_3
SGTH1	30 SiO_2-30 GeO_2-20($CaO + Li_2O$)-5Nb_2O_5-15BaO -1Ho_2O_3-0.5Tm_2O_3
SGTH2	30 SiO_2-30 GeO_2-20($CaO + Li_2O$)-5Nb_2O_5-15BaO -1Ho_2O_3-1.5Tm_2O_3

Table 2. Physical and Thermal Properties of Silicate-Germanate Glasses

Sample	Parameter	Value
S0	Density ρ (g/cm^3)	3.36
	Refractive index n_D	1.61
SG	Density ρ (g/cm^3)	3.56
	Refractive index n	1.69
SGTH	Refractive index n	1.70
	T_g (°C)	585
	T_x (°C)	740
	ΔT (°C)	155
	Sample thickness (mm)	1.50

B. Raman Spectrum

In the last decades, the structure of niobium silicate glasses [30,31] and alkali germanaosilicate glasses [32] has been reported by the Raman spectroscopic technique. However, few papers, to the best of our knowledge, have reported on the Raman spectra of niobium silicate-germanate glass. Figure 1 presents the vibrational spectra of an investigated silicate-germanate glass sample. It can be seen that the maximum phonon energy of the present sample is located at 804 cm^{-1}, which is lower than that of sodium germanosilicate glass (862 cm^{-1}) [33]. For the sake of detailed analysis, the Gaussian deconvolution procedure is utilized to fit multipeaks [34], and the result is showed in Fig. 1. It can be found that the bands of five peaks are around at 325, 552, 784, 804, and 973 cm^{-1}. According to the reported literatures, the low frequency region at around ~325 cm^{-1} is related to the chains of GeO_4 tetrahedra connected by six coordinated Ge units within the network [32]. Meanwhile, the weak peak at around ~552 cm^{-1} was observed, which has been attributed to the presence of germania, related to the Ge-O-Nb bonds, a structural network formed by GeO_4 tetrahedra and NbO_6 octahedra according to [35,36]. In the high-frequency region, the band at 784 cm^{-1} is assigned to NbO_6 octahedra [36]. The latter intensity band centered near 804 cm^{-1} should be assigned to the Nb-O bonds because, as the polarizability of Nb-O bonds is higher than that of Si-O bonds on the Raman spectra, the bands related to Si-O vibrations usually cannot be seen [31]. Compared with the structure of SiO_2 glass [37] and the alkali germanate compositions [32], the new shoulder is observed at ~973 cm^{-1} in the silicate-germanate glass, which should be related to the vibrational modes of Ge-O-Si linkages [35].

C. Absorption Spectra

In order to better understand the properties of glass, some important optical parameters were calculated for our samples. Figure 2 shows optical absorption spectra of Tm^{3+} single doped, and Tm^{3+}/Ho^{3+} co-doped silicate-germanate glasses at room temperature in the wavelength range from 400 to 2200 nm. The length of samples is 10 mm for the measurement

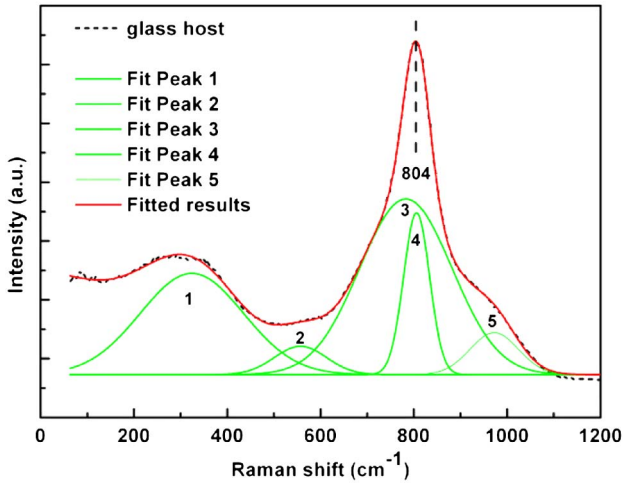

Fig. 1. Deconvolution of Raman spectrum of SG glass using symmetric Gaussian functions.

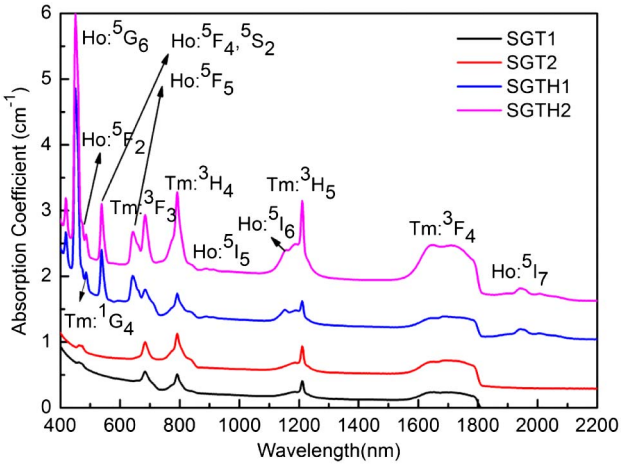

Fig. 2. Absorption spectra of Tm^{3+} single-doped and Tm^{3+}/Ho^{3+} co-doped silicate-germanate glasses in the range of 400–2200 nm.

of the absorption spectra. The spectra shapes of single-doped or co-doped glass samples are similar, and the absorption intensity is proportional to the mol content of Tm^{3+} and Ho^{3+} ions.

From the absorption spectra, several inhomogeneously broadened absorption peaks can be observed, which are assigned to the transition from the ground-state level to the excited states of 4f configuration of Tm^{3+} and Ho^{3+} ions, respectively. Some important absorption bands are labeled in the spectra. It can be seen that the 808 or 980 nm LD is not applicable to Ho^{3+} ions. Nevertheless, levels $^3H_4$ of the Tm^{3+} ions can be excited at 808 nm. The intense absorption band centered at nearly 800 nm of the Tm^{3+}/Ho^{3+} co-doped sample from absorption curve, which indicates Tm^{3+} can function as an absorber to increase the absorption of the 808 nm pumping energy. Additionally, in comparison to single-doped and co-doped glass samples, it can be found that the shape and peak positions of each transition are similar, and there is no shift of the absorption peaks. This result indicates that there is no apparent cluster in the local ligand field, and both Ho^{3+} and Tm^{3+} ions are homogeneously incorporated into the glassy network. Meanwhile, Figure 2 shows the absorption peak intensity with Tm^{3+} ions at different concentrations, in which a significant increase of absorption with increased Tm^{3+} ions concentrations is clearly observed when concentrations of Ho_2O_3 remained constant.

D. J-O Analysis and Radiative Properties

To the best of our knowledge, J-O theory [38,39] has been often used to discuss the radiative properties of rare-earth ions within the host matrix from the absorption spectra. According to J-O theory, the J-O intensity parameters Ω_2, Ω_4, and Ω_6 for 4f–4f transitions of Ho^{3+} ions in the glass samples were computed from the measured absorption spectra. Afterward, these parameters Ω_t ($t = 2, 4, 6$) were used to evaluate radiative properties of the main laser emitting levels of Ho^{3+} in silicate-germanate glass, such as radiative transition probability (A_{rad}), fluorescence branching ratios (β), and radiative lifetime (τ_{rad}). The parameters Ω_λ are important for the investigation of the local structure and bonding in the vicinity of rare-earth ions. The J-O intensity parameters of glass in this paper are compared with those obtained from

Table 3. J-O intensity Parameters (Ω_λ, $\lambda = 2, 4, 6$) ($\times 10^{-20}$ cm^2) of Ho^{3+} Ions in Various Glass Hosts

Samples	Ω_2	Ω_4	Ω_6	Trend	Reference
SGTH2	6.5	2.61	0.33	$\Omega_2 > \Omega_4 > \Omega_6$	This work
Tellurite	5.21	2.28	2.18	$\Omega_2 > \Omega_6 > \Omega_4$	[14]
Silicate	5.20	1.80	1.20	$\Omega_2 > \Omega_4 > \Omega_6$	[40]
Phosphate	3.33	3.01	0.61	$\Omega_2 > \Omega_4 > \Omega_6$	[40]
Fluoride	1.86	1.90	1.32	$\Omega_2 > \Omega_6 > \Omega_4$	[41]
Fluorophosphate	3.23	2.71	1.82	$\Omega_2 > \Omega_4 > \Omega_6$	[42]
Germanate	6.60	1.75	0.99	$\Omega_2 > \Omega_4 > \Omega_6$	[43]

various other Ho^{3+} doped glasses, as listed in Table 3. It should be noted that the five absorption bands—$^5I_6$, $^5F_5$, $^5F_4 + {}^5S_2$, $^5F_1 + {}^5G_6$, and $^5G_5$—were used for the calculation in this process because the transition $^5I_8 \rightarrow {}^5I_7$ has a substantial magnetic dipole component. From Table 3, it is observed that the oxide glasses have large Ω_2 and small Ω_6 values. The Ω_2 parameter of silicate-germanate glass follows the trend $\Omega_2 > \Omega_4 > \Omega_6$. This trend is consistent with the one observed for other glasses, such as silicate, germanate, fluorophosphate, and phosphate glasses; however, it differs from those of fluoride and tellurite glasses, as shown in Table 3. The root mean square deviation δ_{rms} was calculated to be 1.31×10^{-6}. According to previous studies, Ω_2 is related with some factors such as the ligand symmetry of host glass, the degree of covalency of the chemical bonds between rare-earth ions and its nearest neighbor atoms of a glass. Ω_4 and Ω_6 are related to the covalency of the medium in which the rare-earth ions are situated. And Ω_6 reflect the bulk properties of the host such as rigidity and viscosity [8], which can be adjusted by the composition or structure of the glass host. It is also found that Ω_2 for Ho^{3+} in this work is larger than that of silicate [40], fluoride [41], fluorophosphate [42], tellurite [14], and phosphate [40] glass hosts. A large Ω_2 value is probably due to relatively high covalency of the chemical bond between rare-earth and oxygen ions. But the value of Ω_2 is smaller than that in germanate [43] glass. Thus the result indicates that ligand asymmetry around the rare-earth ions in Tm^{3+}/Ho^{3+} co-doped germanate glass is stronger than those in silicate-germanate glass. The smaller the Ω_6 value is, the stronger covalence between anions and rare-earth ions. It can be seen clearly that the Ω_6 of studied glass is smaller than that of various other glasses, as shown in Table 3. The J-O analysis indicated a strong asymmetry and covalent environment between the rare-earth ions and the ligand in the present matrix.

Furthermore, the spontaneous transition properties of the Ho^{3+} are shown in Table 4, including the spontaneous transition probability A_{rad}, branching ratio β, and radiative lifetime τ_{rad} of different emission states of Ho^{3+} ions in silicate-germanate glass, which were evaluated using the three intensity parameters through J-O theory. Table 4 shows that the values of A_{rad} for the Ho^{3+}:$^5I_7 \rightarrow {}^5I_8$ transition and τ_{rad} of the $^5I_7$ level of Ho^{3+} are 103.46 s^{-1} and 9.67 ms, respectively. The A_{rad} value is larger than that of germanate, phosphate [41], silicate [44], and fluorophosphates [45] glasses. Higher A_{rad} is beneficial in achieving intense infrared emissions. Consequently, this silicate-germanate glass can be considered as an appropriate host glass to achieve 2 μm laser from the Ho^{3+}:$^5I_7 \rightarrow {}^5I_8$ transition.

Table 4. Spontaneous Transition Probability A_{rad}, Branching Ratio β, and Radiative Lifetime τ_{rad} for Different Excited Levels of Ho^{3+} in Silicate-Germanate Glass

Transition	Energy (cm^{-1})	A_{rad} (s^{-1})	β (%)	τ_{rad} (ms)
$^5I_7 \rightarrow {}^5I_8$	5139	103.46	100	9.67
$^5I_6 \rightarrow {}^5I_8$	8681	155.77	84.20	5.41
$^5I_6 \rightarrow {}^5I_7$	3321	29.23	–	–
$^5I_5 \rightarrow {}^5I_8$	11187	61.66	37.51	6.08
$^5I_5 \rightarrow {}^5I_7$	6046	82.36	–	–
$^5I_5 \rightarrow {}^5I_6$	2726	20.37	–	–
$^5F_5 \rightarrow {}^5I_8$	15528	2039.53	77.33	0.38
$^5F_5 \rightarrow {}^5I_7$	10384	1215.8	–	–
$^5F_5 \rightarrow {}^5I_6$	7067	178.8	–	–
$^5F_5 \rightarrow {}^5I_5$	4342	14.4	–	–

E. Fluorescence Spectra

Figure 3 shows Tm^{3+}/Ho^{3+} co-doped silicate-germanate glass fluorescence spectra in the range of 1600–2200 nm when excited by 808 nm LD at room temperature. From Fig. 3, it can be seen clearly that two emission peaks are centered near at 1.8 and 2 μm, which correspond to the Tm^{3+}:$^3F_4 \rightarrow {}^3H_6$ and Ho^{3+}:$^5I_7 \rightarrow {}^5I_8$ transition, respectively. Moreover, the 1.8 and 2 μm fluorescent intensity is in direct proportion to the Tm_2O_3 concentration, while, compared with the 2 μm emission, the emission intensity of 1.8 μm increased relatively little. Due to the intense energy transferring (ET) between the $^3F_4$ state of Tm^{3+} and Ho^{3+}:$^5I_7$ state and cross-relaxation (CR) of adjacent Tm^{3+} ions.

In order to explain the mechanism of strong 2 μm luminescence, Fig. 4 shows the simplified energy level diagrams of Tm^{3+} and Ho^{3+} ions identified from the absorption spectra. The locations of the energy levels are similar to those reported previously for bismuthate [9] and tellurite [11] glass hosts. And the detailed energy transfer paths between the two rare-earth ions can be illustrated. In Fig. 4, the start state $^3H_6$ of Ho^{3+} ions are initially excited to the excited state of the Ho^{3+}:$^3F_4$ level when Tm^{3+}/Ho^{3+} co-doped glass is pumped by 808 nm LD. Afterward, part of the ions of Tm^{3+} in the $^3H_4$ state drop down to the $^3F_4$ state, then the Tm^{3+}:$^3F_4$ level decays to the $^3H_6$ level emitting 1.8 μm fluorescence. While

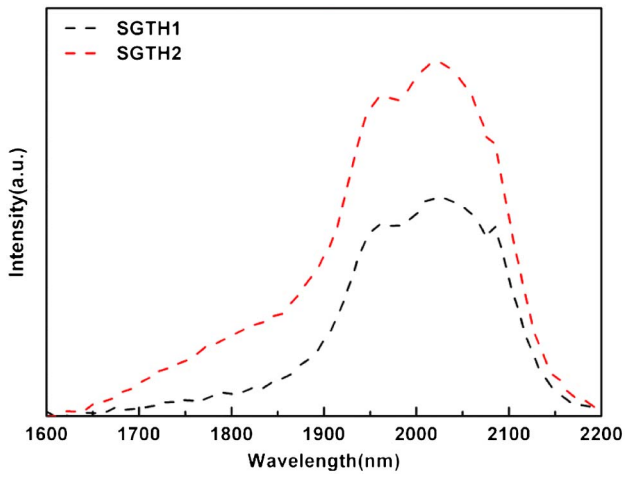

Fig. 3. Fluorescence spectra of the Tm^{3+}/Ho^{3+} co-doped silicate-germanate glasses.

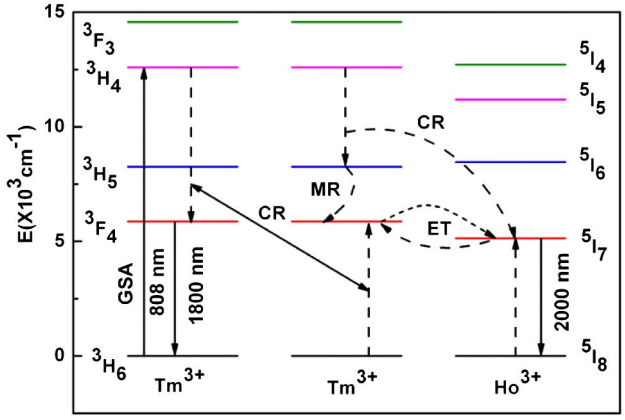

Fig. 4. Energy level diagrams and energy transfer sketch map of Tm^{3+} and Ho^{3+} ions.

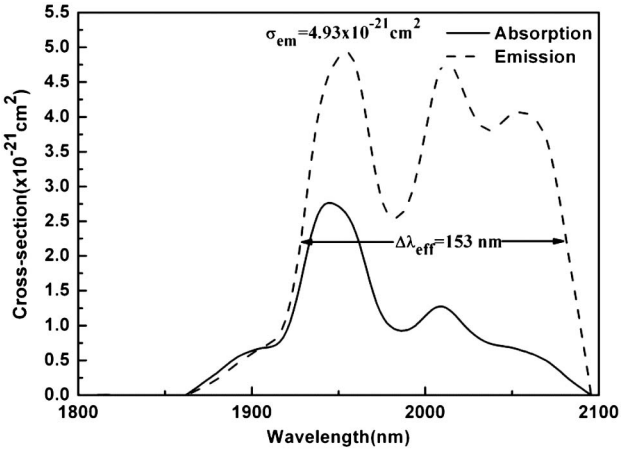

Fig. 5. Emission cross sections of silicate-germanate glasses doped with 1.5 mol% Tm_2O_3 and 1 mol% Ho_2O_3.

most of the excited Tm^{3+} ions in $^3H_4$ states are excited from the $^3H_6$ ground state to $^3F_4$ state via CR between Tm^{3+}:$^3H_4$ level and Tm^{3+}:$^3H_6$ level and multiphonon relaxation (MR) process. Tm^{3+} ions in the $^3F_4$ state transfer energy to the Ho^{3+} ions in $^5I_7$ state via the ET process. After that, once the Ho^{3+}:$^5I_7$ state is populated, the 2 μm emission via Ho^{3+}:$^5I_7 \rightarrow {}^5I_8$ transition takes place. The detail transfer mechanism is described as follows:

$$^3H_6(Tm^{3+}) + h\nu(808\ \text{nm}) \rightarrow {}^3H_4(Tm^{3+})\ \text{(GSA)}$$

$$^3H_4(Tm^{3+}) + {}^3H_6(Tm^{3+}) \rightarrow {}^3F_4(Tm^{3+}) + {}^3F_4(Tm^{3+})\ \text{(CR)}$$

$$^3F_4(Tm^{3+}) \rightarrow {}^3H_6(Tm^{3+}) + h\nu'(1.8\ \mu\text{m})\ \text{(emission)}$$

$$^3F_4(Tm^{3+}) + {}^5I_8(Ho^{3+}) \rightarrow {}^3H_6(Tm^{3+}) + {}^5I_7(Ho^{3+})\ \text{(ET)}$$

$$^5I_7(Ho^{3+}) \rightarrow {}^5I_8(Ho^{3+}) + h\nu'(2\ \mu\text{m})\ \text{(emission)}$$

F. Absorption and Emission Cross Sections

The absorption and emission cross sections are two vital spectroscopic parameters and related to the optical gain of a laser material. The emission cross section (σ_{em}) of Ho^{3+}:$^5I_7 \rightarrow {}^5I_8$ can be derived from Eq. (1) by using the McCumber theory [46]:

$$\sigma_{em}(\lambda) = \sigma_{abs}(\lambda) \times \frac{Z_l}{Z_u} \times \exp\left[\frac{hc}{kT} \times \left(\frac{1}{\lambda_{ZL}} - \frac{1}{\lambda}\right)\right], \quad (1)$$

where Z_l/Z_u is the partition functions ratio involved in the considered optical transition. Here T is the room temperature, k is the Boltzmann constant, and λ_{ZL} is the wavelength for the transition between the lower Stark sublevels of the emitting multiplets and the lower Stark sublevels of the receiving multiplets. The σ_{abs} is the absorption cross section of Tm^{3+}/Ho^{3+} co-doped sample, which is calculated from the absorption spectra by using Eq. (2):

$$\sigma_{abs}(\lambda) = \frac{2.303\ \log(I_0/I)}{Nl}, \quad (2)$$

where N is the concentration of Ho^{3+} ions, l is the thickness of the glass samples, and $\log(I_0/I)$ is the absorptivity from absorption spectra, respectively.

Moreover, the emission cross section (σ_{em}) also can be calculated from the fluorescence spectrum by the Fuchtbauer–Ladenburg equation in Eq. (3):

$$\sigma_{em}(\lambda) = \frac{\lambda^4 A_{rad}}{8\pi c n^2} \times \frac{\lambda I(\lambda)}{\int \lambda I(\lambda) d\lambda}, \quad (3)$$

where λ is the emission wavelength, A_{rad} is the spontaneous radiative transition probability of Ho^{3+}:$^5I_7 \rightarrow {}^5I_8$ transition, c is the velocity of light in vacuum, n is the refractive index of glass host, $I(\lambda)$ is the fluorescence intensity, and $\int I(\lambda)d\lambda$ is the integrated fluorescence intensity.

Figure 5 shows the absorption and emission cross sections for Ho^{3+}:$^5I_8 \rightarrow {}^5I_7$ transition based on McCumber theory. According to the figure, it can be found that the peak absorption cross section of Ho^{3+}:$^5I_8 \rightarrow {}^5I_7$ transition in silicate-germanate glass reaches 2.77×10^{-21} cm^2 near 1946 nm, and the emission cross section of Ho^{3+} is 4.78×10^{-21} cm^2 at 2014 nm, respectively. The value of emission cross section is a little larger than that of fluoride glass [47] and silicate glass [44] but smaller than the value of germanate glass [48]. Compared with silicate ($n = 1.48$) or phosphate ($n = 1.52$) glasses [22], the prepared silicate-germanate glass has a high refractive index ($n = 1.7$), the higher refractive index of the host glass induces the higher emission cross section of Ho^{3+}, due to the electric dipole transitions of rare-earth ions increasing as the refractive index of the glass increases [22]. It is worth noting that the emission cross section is as large as possible to obtain high gain for a laser medium [49]. Thus, Tm^{3+}/Ho^{3+} co-doped silicate-germanate glass could be a suitable candidate matrix for 2 μm optical fiber amplifier.

G. Laser Spectroscopic Properties

Table 5 shows the emission cross-section σ_e^{peak} and the FWHM of the emission peak of Ho^{3+}:$^5I_7 \rightarrow {}^5I_8$ transition in different glass hosts. The $\sigma_e^{peak} \times$ FWHM is an important parameter in which to characterize the bandwidth properties of the optical amplifier materials, the larger value of which represents the wider gain bandwidth and the higher gain character [50]. The value of $\sigma_e^{peak} \times \tau_m$ is another parameter that can be applied to evaluate the gain of bandwidth [51]. As the results show in Table 5, $\sigma_e^{peak} \times$ FWHM is 731.34×10^{-28} cm^3 and $\sigma_e^{peak} \times \tau_m$ is 46.22×10^{-21} cm$^2 \cdot$ ms in this work, respectively. Those values are much larger than those of various glasses, excluding fluoride [8] glass, as shown in Table 5. Therefore, it is desirable that the Tm^{3+}/Ho^{3+} co-doped

Table 5. Peak Cross Section σ_e^{peak}, FWHM, Radiative Lifetime τ_m, σ_e^{peak} × FWHM and σ_e^{peak} × τ_m of $^5I_7 \rightarrow {}^5I_8$ Transition of Ho^{3+} in Different Glass Samples

Glasses	FWHM(nm)	σ_e^{peak} (10^{-21} cm^2)	τ_m (ms)	σ_e^{peak} × FWHM (10^{-28} cm^3)	σ_e^{peak} × τ_m (10^{-21} $cm^2 \cdot ms$)	Reference
SGTH2	153	4.78	9.67	731.34	46.22	This paper
Silicate	82	7.0	0.32	574	2.24	[8]
Germanate	84	4.0	0.36	336	1.44	[8]
Gallate	141	3.8	8.2	535.8	31.16	[8]
Fluoride	118	5.3	26.7	625	141.51	[8]
Tellurite	–	10.7	2.2	–	23.54	[11]

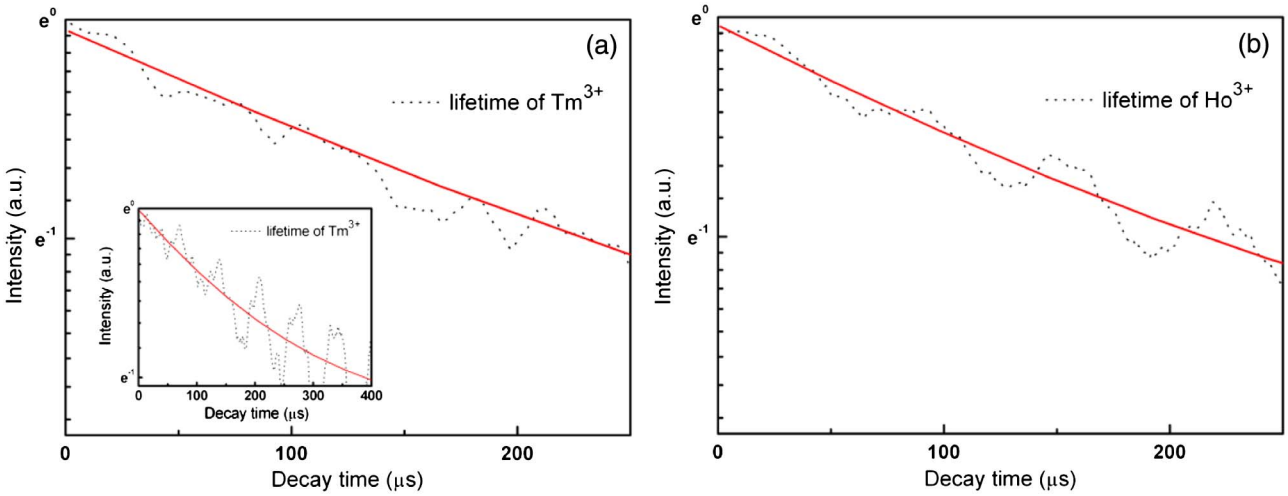

Fig. 6. (a) Fluorescence decay curve of Tm^{3+}/Ho^{3+} co-doped glass sample from Tm^{3+}:$^3F_4 \rightarrow {}^3H_6$. Inset shows the decay curve of Tm^{3+} singly doped glass sample. (b) Fluorescence decay curve of Tm^{3+}/Ho^{3+} co-doped glass samples from Ho^{3+}:$^5I_7 \rightarrow {}^5I_8$.

silicate-germanate glass should become a suitable host material to be used as a candidate for broadband optical amplifiers or a 2 μm laser.

H. Energy Transfer Efficiency

Figure 6 shows the decay curves of glass samples. By using the lifetime value of the Tm^{3+}:$^3F_4$ energy level, the energy transfer efficiency from Tm^{3+}:$^3F_4$ to Ho^{3+}:$^5I_7$ in silicate-germanate glass can be estimated as follows [52]:

$$\eta = 1 - \frac{\tau_{Tm/Ho}}{\tau_{Tm}}. \tag{4}$$

The energy transfer rate was found to be connected to the effective lifetime, which can be defined as [53]

$$W_{ET} = \frac{1}{\tau_{Tm/Ho}} - \frac{1}{\tau_{Tm}}, \tag{5}$$

where $\tau_{Tm/Ho}$ and τ_{Tm} are the lifetimes of Tm^{3+} ions in Tm^{3+}/Ho^{3+} co-doped and Tm^{3+} single-doped glass samples, respectively.

The quantum efficiency (Q.E.) was determined for the Ho^{3+}:$^5I_7 \rightarrow {}^5I_8$ in the Tm^{3+}/Ho^{3+} co-doped silicate-germanate glass samples, as [54]

$$\text{Q.E.} = \frac{\tau_{obs}}{\tau_{rad}}, \tag{6}$$

where τ_{obs} and τ_{rad} are the measured luminescence lifetime and radiative lifetime of Ho^{3+} ions, respectively.

According to Fig. 6, it can be found that the fluorescence lifetime of Tm^{3+}:$^3F_4$ becomes shorter as Ho^{3+} ions co-dope into the Tm^{3+}-ions-doped sample. This indicates that energy transfer occurred between the Tm^{3+}:$^3F_4$ and Ho^{3+}:$^5I_7$ level. And the lifetimes of Tm^{3+}:$^3F_4$ with and without Ho^{3+} are 222 and 399 μs, and the measured lifetime of Ho^{3+}:$^5I_7$ in Tm^{3+}/Ho^{3+} co-doped silicate-germanate glass is 210 μs, respectively. Thus, the energy-transfer efficiency and energy-transfer rate between Tm^{3+} and Ho^{3+} ions in silicate-germanate glass were calculated, which is 52% and 2760.55 s^{-1}, respectively. The efficiency value for energy transfer to Ho^{3+} from Tm^{3+} ions of the present glass is larger than that of fluorozircoaluminate glass [47]. The high value of energy transfer efficiency implied the high sensitization efficiency of Tm^{3+}/Ho^{3+} in co-doped silicate-germanate glass here, which is helpful for development of the 2 μm laser. The Q.E. of the Ho^{3+}:$^5I_7 \rightarrow {}^5I_8$ transition is 2.17%, which is higher than that of silicate glass [43]. The results demonstrate that the incorporation of Tm^{3+} as a sensitizer through efficient energy transfer from Tm^{3+} ($^3F_4$) to Ho^{3+} ($^5I_7$) under 808 nm excitation can be obtained by 2 μm emission efficiently in the silicate-germanate glass.

4. CONCLUSION

In summary, Tm^{3+} doped and Tm^{3+}/Ho^{3+} co-doped silicate-germanate glasses were prepared. We successfully obtain the

2 μm luminescence of Ho^{3+} in Tm^{3+}/Ho^{3+} co-doped silicate-germanate glass under excitation of an 808 nm LD. The Tm^{3+}/Ho^{3+} co-doped silicate-germanate glasses exhibited good thermal stability. According to the Raman spectrum, the structure features of the present silicate-germanate glass appears to contain alternating SiO_4 tetrahedra, GeO_4 tetrahedra, and NbO_6 octahedra. The J-O intensity parameters, transition properties, branching ratios, and radiative lifetimes have been determined. The value of FWHM (153 nm) was recorded in Tm^{3+}/Ho^{3+} co-doped SGTH2 glass at room temperature when pumped by 808 nm LD. Tm^{3+}/Ho^{3+} co-doped silicate-germanate glasses exhibit large $\sigma_e^{peak} \times FWHM$ (up to 731.34×10^{-28} cm^3), which indicates that the present glass has better gain properties as laser material. Furthermore, a large stimulated emission cross section and gain coefficient for Ho^{3+}:$^5I_7 \rightarrow {}^5I_8$ transition of Tm^{3+}/Ho^{3+} co-doped silicate-germanate glasses indicate that these glasses find applications in mid-infrared laser devices at ~2 μm. The energy transfer efficiency and rate were calculated to be 52% and 2760.55 s^{-1}, respectively. The Q.E. of the $^5I_7 \rightarrow {}^5I_8$ transition of Ho^{3+} is 2.17%. As a result, Tm^{3+}/Ho^{3+} co-doped silicate-germanate glass with good spectroscopic properties might be a promising candidate as a host for developing laser or optical amplifier devices.

Funding. Natural Science Foundation of Zhejiang Province of China (LY15E020009, LY13F050003, LR14E020003); National Natural Science Foundation of China (NSFC) (61370049, 61308090, 61405182, 51172252, 51372235, 51472225); International Science & Technology Cooperation Program of China (2013DFE63070); Public Technical International Cooperation Project of the Science Technology Department of Zhejiang Province (2015c340009).

REFERENCES

1. B. Richards, A. Jha, Y. Tsang, and W. Sibbett, "Tellurite glass lasers operating close to 2 μm," Laser Phys. Lett. **7**, 177–193 (2010).
2. G. J. Koch, M. Petros, J. Yu, and U. N. Singh, "Precise wavelength control of a single-frequency pulsed Ho:Tm:YLF laser," Appl. Opt. **41**, 1718–1721 (2002).
3. K. Scholle, E. Heumann, and G. Huber, "Single mode tm and Tm, Ho: LuAG lasers for LIDAR applications," Laser Phys. Lett. **1**, 285–290 (2004).
4. R. Cao, M. Peng, L. Wondraczek, and J. Qiu, "Superbroad near-to-mid-infrared luminescence from Bi_5^{3+} in $Bi_5(AlCl_4)_3$," Opt. Express **20**, 2562–2571 (2012).
5. S. Li, P. Wang, H. Xia, J. Peng, L. Tang, Y. Zhang, and H. Jiang, "Tm^{3+} and Nd^{3+} singly doped $LiYF_4$ single crystals with 3–5 μm mid-infrared luminescence," Chin. Opt. Lett. **12**, 021601 (2014).
6. A. Hemming, S. Bennetts, N. Simakov, A. Davidson, J. Haub, and A. Carter, "High power operation of cladding pumped holmium-doped silica fiber lasers," Opt. Express **21**, 4560–4566 (2013).
7. C. Liu, C. Ye, Z. Luo, H. Cheng, D. Wu, Y. Zheng, Z. Liu, and B. Qu, "High-energy passively *Q*-switched 2 μm Tm^{3+}-doped double-clad fiber laser using graphene-oxide–deposited fiber taper," Opt. Express **21**, 204–209 (2013).
8. L. Yi, M. Wang, S. Feng, Y. Chen, G. Wang, L. Hu, and J. Zhang, "Emission properties of Ho^{3+}: $^5I_7 \rightarrow {}_5I^8$ transition sensitized by Er^{3+} and Yb^{3+} in fluorophosphates glasses," Opt. Mater. **31**, 1586–1590 (2009).
9. B. S. Yong, H. T. Lim, Y. G. Choi, Y. S. Kim, and J. Heo, "2.0 μm emission properties and energy transfer between Ho^{3+} and Tm^{3+} in $PbO-Bi_2O_3-Ga_2O_3$ glasses," J. Am. Ceram. Soc. **83**, 787–791 (2000).
10. Y. Ju, W. Liu, B. Yao, T. Dai, J. Wu, J. Yuan, J. Wang, X. Duan, and Y. Wang, "Diode-pumped tunable single-longitudinal-mode Tm, Ho:YAG twisted-mode laser," Chin. Opt. Lett. **13**, 111403 (2015).
11. G. Gao, L. Hu, H. Fan, G. Wang, K. Li, S. Feng, S. Fan, H. Chen, J. Pan, and J. Zhang, "Investigation of 2.0 μm emission in Tm^{3+} and Ho^{3+} co-doped TeO_2-ZnO-Bi_2O_3 glasses," Opt. Mater. **32**, 402–405 (2009).
12. L. Kong, G. Xie, P. Yuan, L. Qian, S. Wang, H. Yu, and H. Zhang, "Passive *Q*-switching and *Q*-switched mode-locking operations of 2 μm Tm:CLNGG laser with MoS_2 saturable absorber mirror," Photo. Res. **3**, A47–A50 (2015).
13. W. Zhang, L. Rong, J. Ren, Y. Jia, and S. Qian, "Judd-Ofelt analysis and mid-infrared emission properties of Ho^{3+}-Yb^{3+} co-doped tellurite oxy-halide glasses," Proc. SPIE **8906**, 89060 (2013).
14. G. Chen, Q. Zhang, G. Yang, and Z. Jiang, "Mid-infrared emission characteristic and energy transfer of Ho^{3+}-doped tellurite glass sensitized by Tm^{3+}," J. Fluoresc. **17**, 301–307 (2007).
15. S. D. Jackson, "The effects of energy transfer upconversion on the performance of Tm^{3+}/Ho^{3+}-doped silica fiber lasers," IEEE Photon. Technol. Lett. **18**, 1885–1887 (2006).
16. Q. Zhang, J. Ding, Y. Shen, G. Zhang, G. Lin, J. Qiu, and D. Chen, "Infrared emission properties and energy transfer between Tm^{3+} and Ho^{3+} in lanthanum aluminum germanate glasses," J. Opt. Soc. Am. B **27**, 975–980 (2010).
17. T. Wei, C. Tian, M. Z. Cai, Y. Tian, X. F. Jing, J. J. Zhang, and S. Q. Xu, "Broadband 2 μm fluorescence and energy transfer evaluation in Ho^{3+}/Er^{3+} codoped germanosilicate glass," J. Quant. Spectrosc. Radiat. Transfer **161**, 95–104 (2015).
18. W. Fan, L. Htein, B. H. Kim, P. R. Watekar, and W. T. Han, "Upconversion luminescence in bismuth-doped germane-silicate glass optical fiber," Opt. Laser Technol. **54**, 376–379 (2013).
19. M. Li, G. Bai, Y. Guo, L. Hu, and J. Zhang, "Investigation on Tm^{3+}-doped silicate glass for 1.8 μm emission," J. Lumin. **132**, 1830–1835 (2012).
20. S. S. Bayya, G. D. Chin, J. S. Sanghera, and I. D. Aggarwal, "Germanate glass as a window for high energy laser systems," Opt. Express **14**, 11687–11693 (2006).
21. Z. Yang, S. Xu, L. Hu, and Z. Jiang, "Thermal analysis and optical transition of Yb^{3+}, Er^{3+} co-doped lead-germanium-tellurite glasses," J. Mater. Res. **19**, 1630–1637 (2004).
22. D. Dorosz, "Rare earth ions doped aluminosilicate and phosphate double clad optical fibres," Bull. Polish Acad. Sci. **56**, 103–111 (2008).
23. G. Bai, L. Tao, K. Li, L. Hu, and Y. H. Tsang, "Enhanced light emission near 2.7 μm from Er-Nd co-doped germanate glass," Opt. Mater. **35**, 1247–1250 (2013).
24. T. Xue, L. Zhang, L. Wen, M. Liao, and L. Hu, "Er^{3+} doped fluorogallate glass for mid-infrared applications," Chin. Opt. Lett. **13**, 081602 (2015).
25. R. Xu, Y. Tian, L. Hu, and J. Zhang, "Broadband 2 μm emission and energy-transfer properties of thulium-doped oxyfluoride germanate glass fiber," Appl. Phys. B **104**, 839–844 (2011).
26. A. Hruby, "Evaluation of glass-forming tendency by means of DTA," J. Phys. B **22**, 1187–1193 (1972).
27. M. G. Drexhage, O. H. EI Bayoumi, and C. T. Moyniyan, "Preparation and properties of heavy-metal fluoride glasses containing ytterbium or lutetium," J. Am. Ceram. Soc. **65**, c168–c171 (1982).
28. Y. Messaddeq and M. Poulain, "Stabilizing effect of aluminium, yttrium and zirconium in divalent fluoride glasses," J. Non-Cryst. Solids **140**, 41–46 (1992).
29. F. Huang, X. Liu, W. Li, L. Hu, and D. Chen, "Energy transfer mechanism in Er^{3+} doped fluoride glass sensitized by Tm^{3+} or Ho^{3+} for 2.7 μm emission," Chin. Opt. Lett. **12**, 051601 (2014).
30. K. Fukumi and S. Sakka, "Coordination state of Nb^{5+} ions in silicate and gallate glasses as studied by Raman spectroscopy," J. Mater. Sci. **23**, 2819–2823 (1988).
31. A. Aronne, V. N. Sigaev, B. Champagnon, E. Fanelli, V. Califano, L. Z. Usmanova, and P. Pernice, "The origin of nanostructuring in potassium niobiosilicate glasses by Raman and FTIR spectroscopy," J. Non-Cryst. Solids **351**, 3610–3618 (2005).
32. H. Verweij, "Raman study of the structure of alkali germanosilicate glasses, Lithium, sodium and potassium digermanosilicate glasses," J. Non-Cryst. Solids **33**, 55–69 (1979).

33. Z. Yang, S. Xu, L. Hu, and Z. Jiang, "Density of Na_2O-(3-x)SiO_2-xGeO_2 glasses related to structure," Mater. Res. Bull. **39**, 217–222 (2004).
34. R. Xu, Y. Tian, L. Hu, and J. Zhang, "Structural origin and energy transfer processes of 1.8 μm emission in Tm^{3+} doped germanate glasses," J. Phys. Chem. A. **115**, 6488–6492 (2011).
35. G. S. Henderson, D. R. Neuville, B. Cochain, and L. Cormier, "The structure of GeO_2-SiO_2 glasses and melts: A Raman spectroscopy study," J. Non-Cryst. Solids **355**, 468–474 (2009).
36. E. V. Kolobkova, "Raman-spectroscopy study of the structure of niobium germanate glasses," Soviet J. Glass Phys. Chem. **13**, 176–181 (1988).
37. K. Awazu and H. Kawazoe, "Strained Si-O–Si bonds in amorphous SiO_2 materials: A family member of active centers in radio, photo, and chemical responses," J. Appl. Phys. **94**, 6243–6262 (2003).
38. B. Judd, "Optical absorption intensities of rare-earth ions," Phys. Rev. **127**, 750–761 (1962).
39. G. Ofelt, "Intensities of crystal spectra of rare-earth ions," J. Chem. Phys. **37**, 511–520 (1962).
40. E. Rukmini and C. K. Jayasankar, "Spectroscopic properties of Ho^{3+} ion in zinc borosulphate glasses and comparative energy level analyses of Ho^{3+} ion in various glasses," Opt. Mater. **4**, 529–546 (1995).
41. B. Peng and T. Lzumitani, "Optical properties, fluorescence mechanisms and energy transfer in Tm^{3+}, Ho^{3+} and Tm^{3+}-Ho^{3+} doped near-infrared laser glasses, sensitized by Yb^{3+}," Opt. Mater. **4**, 797–810 (1995).
42. K. Binnemans, R. Deun, C. Walrand, and J. Adam, "Spectroscopic properties of trivalent lanthanide ions in fluorophosphates glasses," J. Non-Cryst. Solids **238**, 11–29 (1998).
43. X. Li, X. Liu, L. Zhang, L. Hu, and J. Zhang, "Emission enhancement in Er^{3+}/Pr^{3+}-codoped germanate glasses and their use as a 2.7 μm laser material," Chin. Opt. Lett. **11**, 121601 (2013).
44. M. Li, X. Liu, Y. Guo, L. Hu, and J. Zhang, "Energy transfer characteristics of silicate glass doped with Er^{3+}, Tm^{3+}, and Ho^{3+} for 2 μm emission," J. Appl. Phys. **114**, 243501 (2013).
45. M. Wang, L. Yi, G. Wang, L. Hu, and J. Zhang, "Emission performance in Ho^{3+} doped fluorophosphates glasses sensitized with Er^{3+} and Tm^{3+} under 800 nm excitation," Solid State Commun. **149**, 1216–1220 (2009).
46. D. E. McCumber, "Einstein relations connecting broadband emission and absorption spectra," Phys. Rev. **136**, A954–A957 (1964).
47. X. Zou and H. Toratani, "Spectroscopic properties and energy transfer in Tm^{3+} singly-and Tm^{3+}/Ho^{3+} doubly-doped glasses," J. Non-Cryst. Solids **195**, 113–124 (1996).
48. R. Xu, M. Wang, Y. Tian, L. Hu, and J. Zhang, "2.05 μm emission properties and energy transfer mechanism of germanate glass doped with Ho^{3+}, Tm^{3+}, and Er^{3+}," J. Appl. Phys. **109**, 053503 (2011).
49. J. Ding, G. Zhao, Y. Tian, W. Chen, and L. Hu, "Bismuth silicate glass: a new choice for 2 μm fiber lasers," Opt. Mater. **35**, 85–88 (2012).
50. Z. Yang, S. Xu, L. Hu, and Z. Jiang, "Thermal analysis and optical properties of Yb^{3+}/Er^{3+}codoped oxyfluoride germanate glasses," J. Opt. Soc. Am. B **21**, 951–957 (2004).
51. D. Shi, Q. Zhang, G. Yang, and Z. Jiang, "Spectroscopic properties and energy transfer in Ga_2O_3-Bi_2O_3-PbO-GeO_2 glasses codoped with Tm^{3+} and Ho^{3+}," J. Non-Cryst. Solids **353**, 1508–1514 (2007).
52. K. Li, Q. Zhang, S. Fan, L. Zhang, J. Zhang, and L. Hu, "Mid-infrared luminescence and energy transfer characteristics of Ho^{3+}/Yb^{3+}codoped lanthanum-tungsten-tellurite glasses," Opt. Mater. **33**, 31–35 (2010).
53. A. Braud, S. Girard, J. L. Doualan, M. Thuau, and R. Moncorgé, "Energy-transfer processes in Yb:Tm-doped KY_3F_{10}, $LiYF_4$, and BaY_2F_8 single crystals for laser operation at 1.5 and 2.3 μm," Phys. Rev. B. **61**, 5280–5292 (2000).
54. L. M. Fortes, L. F. Santos, M. C. Goncalves, R. M. Almeida, M. Mattarelli, M. Montagna, A. Chiasera, M. Ferrari, A. Monteil, S. Chaussedent, and G. C. Righini, "Er^{3+} ion dispersion in tellurite oxychloride glasses," Opt. Mater. **29**, 503–509 (2007).